Supporting Information

The Main Factor that Determines the Formation-Efficiencies of Photochemically Derived One-Electron-Reduced Species

Naoki Hosokawa,[a] Kyohei Ozawa,[a] Kazuhide Koike,[b] Yusuke Tamaki[c] and Osamu Ishitani*[d]

[a] Department of Chemistry, School of Science, Institute of Science Tokyo (Tokyo Institute of Technology), 2-12-1-NE-2 O-okayama, Meguro-ku, Tokyo 152-8550, Japan.
[b] National Institute of Advanced Industrial Science and Technology, Onogawa 16-1, Tsukuba, Ibaraki 305-8569, Japan.
[c] National Institute of Advanced Industrial Science and Technology, 4-2-1 Nigatake, Miyaginoku, Sendai, Miyagi 983-8551, Japan.
[d] Department of Chemistry, Graduate School of Advanced Science and Engineering, Hiroshima University, 1-3-1 Kagamiyama, Higashi-Hiroshima, Hiroshima 739 8526, Japan.

Experimental

General procedures

^{1}H NMR spectra were recorded in chloroform-*d*, acetonitrile-d_3, or acetone-d_6 on JEOL ECA400II and Bruker Ascend 400 (400 MHz) spectrometers. The residual protons of the deuterated solvents were used as internal standards for ^{1}H NMR spectroscopy, whereas the phosphorus and fluorine signals of PF_6^- were used as the internal standard for ^{31}P and ^{19}F NMR spectroscopy. ESI-MS was performed using a Shimadzu LCMS-2010A system with acetonitrile as the mobile phase. Cyclic voltammograms (CV traces) were obtained using tetraethylammonium tetrafluoroborate (Et_4NBF_4) (0.1 M) as the supporting electrolyte under Ar on a BAS CHI760Es electrochemical analyser. Ag/$AgNO_3$ (0.01 M) was used as the reference electrode, platinum (Pt) was used as the counter electrode, and glassy carbon (diameter: 3 mm) was used as the working electrode. The scan rate was set to 200 mV s^{-1}. The acquired CV traces were adjusted to the ferrocene reference potential using the measured half-wave potential of ferrocene in DMA (+0.94 V vs. Ag/$AgNO_3$). DMA was dried over 4 Å molecular sieves and distilled under reduced pressure. Et_4NBF_4 was recrystallised twice from acetonitrile and ethyl acetate and then dried in vacuo at 100 °C overnight before use. All other reagents were of reagent grade and were used without further purification. BIH and the PF_6^- salts of $[Re\{P(OMe)_3\}_2]^+$, $[Re\{P(OEt)_3\}_2]^+$, $[Re(PPh_3)_2]^+$, $[Re(PEt_3)_2]^+$, $[Ir(dFCF_3ppy)_2(bpy)]^+$, and $[Ir(piq)_2(dmb)]^+$ were synthesised according to literature procedures.[1-6]

Photophysical properties

UV-vis absorption spectra were recorded using a JASCO V-670, V-565, or Photal MCPD-9800 spectrophotometer (Ohtsuka Electronics Co., Ltd.). Emission spectra were recorded using a HORIBA Fluorolog-3 system equipped with an NIR-PMT R5509-43 detector. Emission quantum yields were determined using a Quantaurus-QY Plus C13534-01 or C10027 (Hamamatsu Photonics) instrument with a Xe arc lamp fitted with a bandpass filter as the excitation light source, along with an A10080-01 monochromator. Emission lifetimes were measured using a HORIBA Jobin Yvon FluoroCube system with time-correlated single-photon counting (TCSPC). Sample solutions for emission-decay and quantum-yield measurements were degassed by freeze-pump-thaw cycling prior to analysis. Emission-quenching experiments were conducted in Ar-saturated solutions containing the complex and BIH. Quenching rate constants (k_q) were obtained from the slopes of Stern–Volmer plots based on the luminescence intensities at various concentrations of BIH. IR absorption spectra were recorded on a JASCO FT/IR-6600 spectrometer. The phosphorescence spectrum of BIH was recorded with 0.05 ms delay after irradiation by using a HORIBA Fluoromax-4 system.

Franck–Condon analysis

Franck–Condon analysis[7] was used to determine the 0-0 transition energy (E_{00}) of each complex from the emission spectra recorded in DMA at low temperatures. Fitting was performed using the following equation:

$$I(\tilde{\nu}) = \sum_{v_M=0}^{5}\sum_{v_L=0}^{5}\left(\frac{E_{00} - v_M\hbar\omega_M - v_L\hbar\omega_L}{E_{00}}\right)^4\left(\frac{S_M{}^{v_M}}{v_M!}\right)\left(\frac{S_L{}^{v_L}}{v_L!}\right) \exp\left[-4\log 2\left(\frac{\tilde{\nu} - E_{00} + v_M\hbar\omega_M + v_L\hbar\omega_L}{\tilde{\nu}_{1/2}}\right)^2\right] \quad (I)$$

where, $I(\tilde{\nu})$ is the normalised emission intensity at wavenumber $\tilde{\nu}$, $\hbar\omega_M$ and $\hbar\omega_L$ are the energies of the high- and low-frequency acceptor modes, respectively, S_M and S_L are the Huang–Rhys parameters for the high- and low-frequency acceptor modes,[8] and $\tilde{\nu}_{1/2}$ is the half-width of the 0-0 vibrational band.

Coulomb terms, w_r and w_p

In order to determine the driving forces for the photoinduced electron transfer ($-\Delta G_{PET}$) and back electron transfer ($-\Delta G_{BET}$) from OERS to $BIH^{\bullet+}$, we used the following Coulomb terms, w_r and w_p. In the photoinduced electron-transfer process, w_r represents the work arising from electrostatic interactions between PS* and BIH, whereas w_p represents that between $PS^{\bullet-}$ and $BIH^{\bullet+}$. In the back-electron-transfer process, w_r corresponds to the electrostatic interaction work between $PS^{\bullet-}$ and $BIH^{\bullet+}$, and w_p corresponds to that between PS and BI. The values of w_r and w_p are given by the following equation;[11]

$$w_r = \frac{z_D z_A e^2}{d\varepsilon}$$

$$w_p = \frac{z_{D^{\bullet+}} z_{A^{\bullet-}} e^2}{d\varepsilon}$$

where, z denotes the charge of the chemical species, d is the distance of electron-transfer, e is the elementary charge, and ε is the permittivity of solvent.

In the case of **$[Re(PR_3)_2]^+$** and **$[Ir(C\hat{}N)_2(N\hat{}N)]^+$**, these electron-transfer processes are charge-shift reactions. Therefore, in the photoinduced electron transfer processes, $z_{D\,(BIH)}$ and $z_{A^{\bullet-}\,(PS^{\bullet-})}$ are both zero, which causes both w_r and w_p to be zero. Likewise, in the back-electron-transfer process, $z_{D\,(PS^{\bullet-})}$ and $z_{A^{\bullet-}\,(BIH)}$ are zero, so w_r and w_p also become zero.

In the case of **$[Os(CF_3bpy)_3]^{2+}$**, the charge of $PS^{\bullet-}$ is +1. Thus, during the photoinduced electron transfer process, only $z_{D\,(BIH)}$ is zero, which makes w_r equal to zero. In the back electron transfer process, $z_{A^{\bullet-}\,(BIH)}$ is zero, making w_p equal to zero. For both w_p in the photoinduced electron-transfer process and w_r in the back-electron transfer process, we used the reported value for the system between $[Os(X_2bpy)_3]^{2+}$ and BIH (0.03 eV)[11].

Flow electrolysis

UV–Vis and IR absorption spectra under bulk-electrolysis conditions were recorded using a flow electrolysis apparatus and an ALS/CHI BAS CHI-720D electrochemical analyser as the potentiostat. UV-Vis absorption spectra were recorded using a Photal MCPD-9800 photodiode array spectrometer, and IR absorption spectra were recorded using a JASCO FT/IR-6600 IR spectrometer. Sample solutions were prepared in DMA containing 0.1 M Et_4NBF_4 as the supporting electrolyte and were bubbled with Ar for over 40 min prior to analysis. The sample solution was pumped at a flow rate of 0.1 mL min^{-1} using a JASCO PU-4180i HPLC pump through a VF-2 electrolysis cell (EC Frontier) and then through a quartz flow cell (1.5 mm light path) for UV-Vis spectroscopy and an IR flow cell with CaF_2 windows (1.5 mm light path) for IR spectroscopy. The flow electrolysis cell was constructed with a carbon felt working electrode, a $Ag/AgNO_3$ (0.01 M) reference electrode, and a Pt-wire counter electrode.

The number of electrons (n) consumed during complex reduction was evaluated using Eq. (II). The reduction current (i) was determined from the plateau observed in the plot of current as a function of the applied potential of the solution, whereas the background current (i_0) was measured using the electrolyte solution devoid of complex. Here [complex], v, and F are the concentration of the metal complex, flow rate, and Faraday constant, respectively.

$$n = \frac{i - i_0}{[\text{complex}] \times v \times F} \qquad \text{(II)}$$

Optically transparent thin-layer electrochemical (OTTLE) cell experiments

The molar extinction coefficient of the OERS (ε_{OERS}) of **$[Os(CF_3bpy)_3]^{2+}$** was determined by observing UV-vis absorption spectral changes using a Photal MCPD-9800 spectrometer, an ALS CHI-620Ex electrochemical analyser, and an optically transparent thin-layer electrochemical (OTTLE) cell (light path length: 1.0 mm, BAS) fitted with a Pt-mesh working electrode, a $Ag/AgNO_3$ (0.01 M) reference electrode, and a Pt-wire counter electrode. The DMA solution containing **$[Os(CF_3bpy)_3]^{2+}$** and 0.1 M Et_4NBF_4 as the supporting electrolyte was degassed with Ar for 20 min prior to any measurement. The absorption spectrum recorded before the second change in absorption shape was assumed to correspond to the OERS and was used to determine ε_{OERS}.

Quantum yield for the formation of the OERS of the PS under steady-state light-irradiation conditions

An Ar-saturated DMA sample solution (4 mL) containing the metal complex and BIH (0.1 M) was prepared. A xenon arc lamp fitted with a band-pass filter (436 nm ± 10 nm, ASAHI SPECTRA) was used as the light source. The sample temperature was maintained at 25.0 ± 0.1 °C using an IWAKI CTS-134A temperature bath. The amount of OERS produced was determined based on changes in the absorption spectrum of the sample solution during irradiation and the molar extinction coefficient (ε_{OERS}) obtained from flow electrolysis or OTTLE measurements.

The light intensity for determining the formation quantum yields of OERS was measured using a $K_3Fe(C_2O_4)_3$ chemical actinometer before the irradiation.[9] The number of absorbed photons was calculated from the measured light intensity and absorbance

at 436 nm of the DMA solution containing the complex and BIH. The quantum yield for OERS formation (Φ_{OERS}) was calculated using the following equation:

$$\Phi_{OERS} = \frac{\text{amount of formed OERS (mol)}}{\text{number of absorbed photon (E)}} \quad \text{(III)}$$

Transient absorption spectroscopy

Transient absorption spectra were recorded using a PicoTAS-ns transient absorption spectroscopy system (UNISOKU Co., Ltd.). A passive Q-sw microchip laser (532 nm, pulse width < 350 nm) was used for transient absorption spectroscopy. An Ar-saturated DMA sample solution containing **$[Re(PEt_3)_2]^+$** (1.0 mM) and BIH (0.1 M) was prepared and bubbled with Ar for 40 min prior to any measurement. The sample solution was circulated using a bimorph pump BPF-465P (NITTO KOHKI Co.) through a quartz optical flow cell (light path: 2 mm).

Synthesis

***cis,trans*−[Re(bpy)(CO)$_2${P(OCH$_2$)$_3$CEt}$_2$](PF$_6$)**

fac-[Re(bpy)(CO)$_3$(CF$_3$SO$_3$)] (102 mg, 0.177 mmol) and P(OCH$_2$)$_3$CEt (282 mg, 1.74 mmol) were dissolved in THF and refluxed for 7 h under Ar in the dark. The mixture was cooled and the solvent was removed under reduced pressure. The resulting crude product was dissolved in saturated methanolic NH_4PF_6 (5 mL) and diethyl ether, hexane, and H_2O were added to precipitate the product. The *fac*-[Re(bpy)(CO)$_3${P(OCH$_2$)$_3$CEt}](PF$_6$) precipitate was purified by recrystallisation from CH_2Cl_2 and diethyl ether. Yield: 101 mg (77.9%).

fac-[Re(bpy)(CO)$_3${P(OCH$_2$)$_3$CEt}](PF$_6$) (101 mg, 0.138 mmol) was dissolved in distilled acetonitrile (100 mL) and degassed by bubbling Ar through the solution for 1.5 h, after which it irradiated with a 500-W high-pressure mercury lamp through a uranyl glass filter for 135 min. The solvent was removed under reduced pressure to yield crude *cis,trans*-[Re(bpy)(CO)$_2${P(OCH$_2$)$_3$CEt}(MeCN)](PF$_6$). The crude product and P(OCH$_2$)$_3$CEt (301 mg, 1.86 mmol) were dissolved in THF (30 mL) and refluxed in the dark for 2 h under Ar. The mixture was cooled and the solvent was removed under reduced pressure to yield a yellow-green solid that was purified by silica-gel column chromatography (CH_2Cl_2/MeOH = 95:5 v/v) and recrystallised from CH_2Cl_2 and diethyl ether. Yield: 54.2 mg (45.2%).

^{1}H NMR (400 MHz, acetone-d_6) δ/ppm: 8.99 (d, J = 5.6 Hz, 2H, bpy−6,6'), 8.72 (d, J = 8.2 Hz, 2H, bpy−3,3'), 8.36 (t, J = 8.2 Hz, 2H, bpy−4,4'), 7.80 (dd, J = 8.2, 5.6 Hz, 2H, bpy−5,5'), 4.18 (t, J = 4.4 Hz, 12H, −POCH_2), 1.20 (q, J = 7.6 Hz, 4H, −CCH_2), 0.74 (t, J = 7.6 Hz, 6H, −CH_3). **^{13}C NMR** (101 MHz, acetonitrile-d_3) δ/ppm: 6.2, 22.8, 35.2, 74.3, 123.8, 127.5, 139.7, 153.5, 155.9 195.6. **^{31}P NMR** (162 MHz, acetonitrile−d_3) δ/ppm: −144.0 (PF_6^-), 106.6 (P(OCH$_2$)$_3$−). **FTIR** (CH_2Cl_2) ν_{CO}/ cm^{-1}: 1984, 1911. **ESI−MS** (MeCN) *m/z* : 723 ([M]$^+$). Anal. Calcd. for $C_{24}H_{30}F_6N_2O_8P_3Re_1 \cdot CH_2Cl_2$: C, 31.52; H, 3.39; N, 2.94. Found: C, 31.41; H, 3.21; N, 3.01.

[Ir(dFCF$_3$ppy)$_2$(tmb)](PF$_6$)

[Ir(dFCF$_3$ppy)$_2$(μ-Cl)]$_2$ (250 mg, 0.168 mmol) and 4,4',5,5'-tetramethyl-2,2'-bipyridine (tmb) (75.7 mg, 0.357 mmol) were dissolved in a 1:1 v/v mixture of MeOH and CH_2Cl_2 (10 mL) and refluxed for 18 h under N_2 in the dark. The mixture was cooled and the solvent was removed under reduced pressure. The resulting crude product was dissolved in saturated methanolic NH_4PF_6 (5 mL) and H_2O was added to precipitate the crude product as a pale-yellow solid that was purified by silica-gel column chromatography (CH_2Cl_2/MeOH = 99:1, v/v) and recrystallised from CH_2Cl_2 and diethyl ether. Yield: 41.4 mg (11.6%).

^{1}H NMR (400 MHz, acetonitrile-d_3) δ/ppm: 8.87 (dd, J = 8.8, 2.8 Hz, 2H), 8.28 (s, 2H), 8.14-8.18 (m, 2H), 7.66-7.69 (m, 2H), 7.60 (s, 2H), 6.75 (ddd, J = 12.8, 9.4, 2.4 Hz, 2H), 5.83 (dd, J = 8.4, 2.4 Hz, 2H), 2.46 (s, 6H), 2.14 (s, 6H) **ESI−MS** (MeCN) *m/z* : 921 ([M]$^+$). Anal. Calcd. for $C_{38}H_{26}F_{16}N_4P_1Ir_1$: C, 42.82; H, 2.46; N, 5.26. Found: C, 43.02; H, 2.36; N, 5.10.

[Os(CF$_3$bpy)$_3$](PF$_6$)$_2$

(NH$_4$)$_2$[OsCl$_6$] (100 mg, 0.23 mmol) and 4,4'-trifluoromethyl-2,2'-bipyridine (CF$_3$bpy) (220 mg, 0.76 mmol) were dissolved in ethylene glycol (10 mL) and refluxed for 4.5 h under Ar in the dark. The reaction mixture was cooled and saturated aqueous NH_4PF_6 (5 mL) was added resulting in the formation of product [Os(CF$_3$bpy)$_3$](PF$_6$)$_2$ as a black solid that was purified by recrystallisation from acetone and diethyl ether. Yield: 116 mg (37%).

^{1}H NMR (400 MHz, acetonitrile-d_3): δ/ppm: 8.94 (s, 6H, CF$_3$bpy-3,3'), 7.87 (d, J = 6.0 Hz, 6H, CF$_3$bpy-6,6'), 7.61 (dd, J = 6.0, 1.6 Hz, 6H, CF$_3$bpy-5,5'). **^{19}F NMR** (376 MHz, acetonitrile-d3) δ/ppm: −65.2 ppm (s, 18F, -CF$_3$), −72.9 ppm (d, J = 706 Hz, 6F, PF_6). **ESI−MS** (MeCN) *m/z*: 534 ([M]$^{2+}$), 1213 ([M + PF_6^-]$^+$). Anal. Calcd. for $C_{36}H_{18}F_{30}N_6P_2Os_1$: C, 31.87; H, 1.34; N, 6.19. Found: C, 31.57; H, 1.21; N, 6.11.

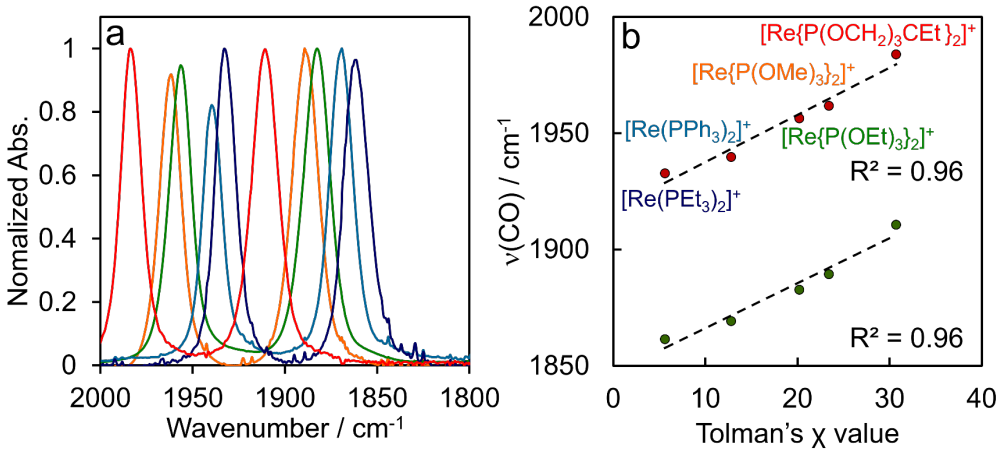

Fig. S1. (a) FTIR spectra of **[Re(PR$_3$)$_2$]$^+$** acquired in CH_2Cl_2 and (b) relationship between two CO stretching vibrations (ν_{CO}) and Tolman's χ value

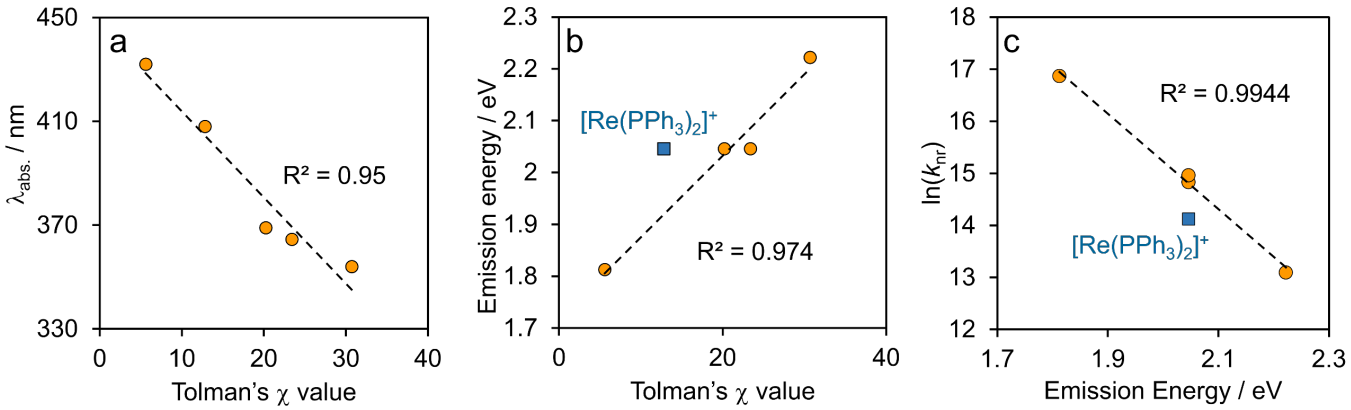

Fig. S2. Plots of (a) λ_{abs} and (b) emission energy as functions of the Tolman's χ value of **[Re(PR$_3$)$_2$]$^+$** measured in DMA. (c) Plot of the logarithm of the radiative decay rate constant (k_{nr}) as a function of **[Re(PR$_3$)$_2$]$^+$** emission energy. The square corresponds to **[Re(PPh$_3$)$_2$]$^+$**.

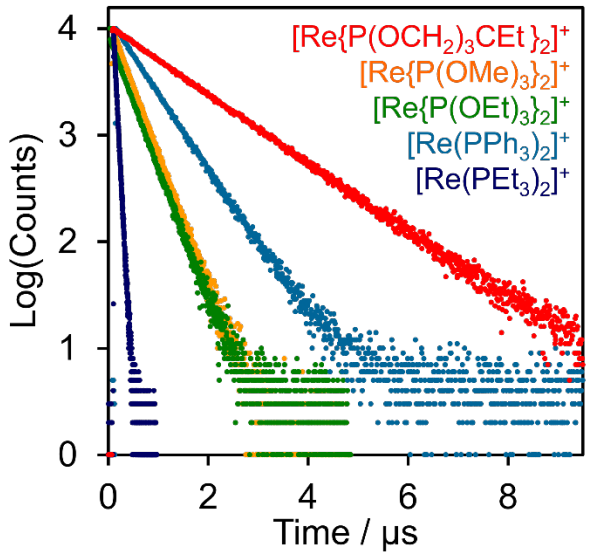

Fig. S3. Emission lifetimes (τ_{em}) of **[Re(PR$_3$)$_2$]$^+$** measured in DMA using the single-photon counting method at room temperature.

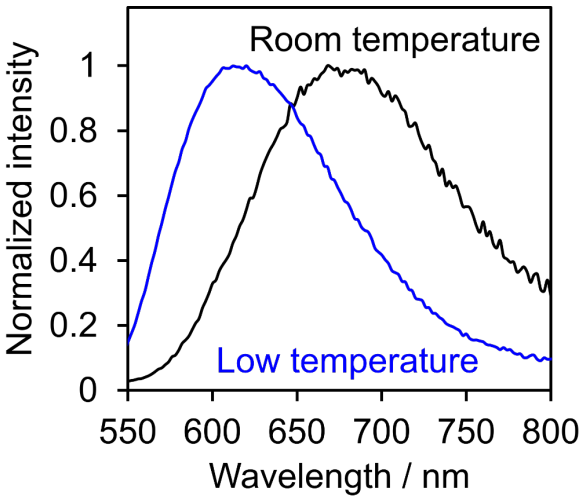

Fig. S4. Emission spectra of **[Re(PEt$_3$)$_2$]$^+$** in DMA at room temperature (black) and low temperature (77K, blue).

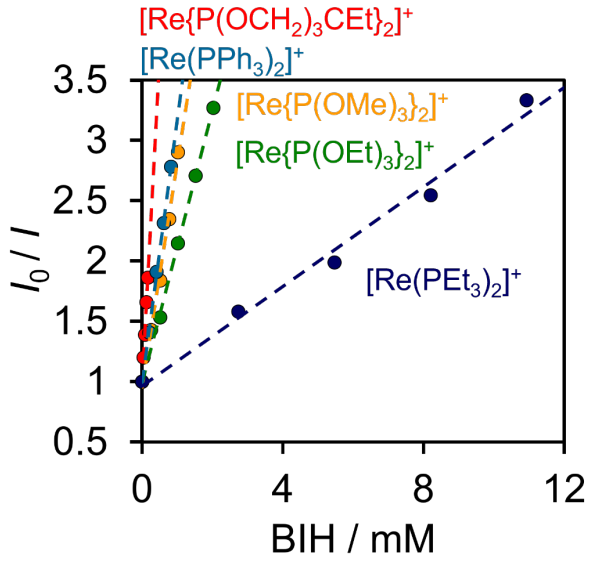

Fig. S5. Stern−Volmer plots for **[Re(PR$_3$)$_2$]$^+$** in DMA in the presence of BIH at various concentrations.

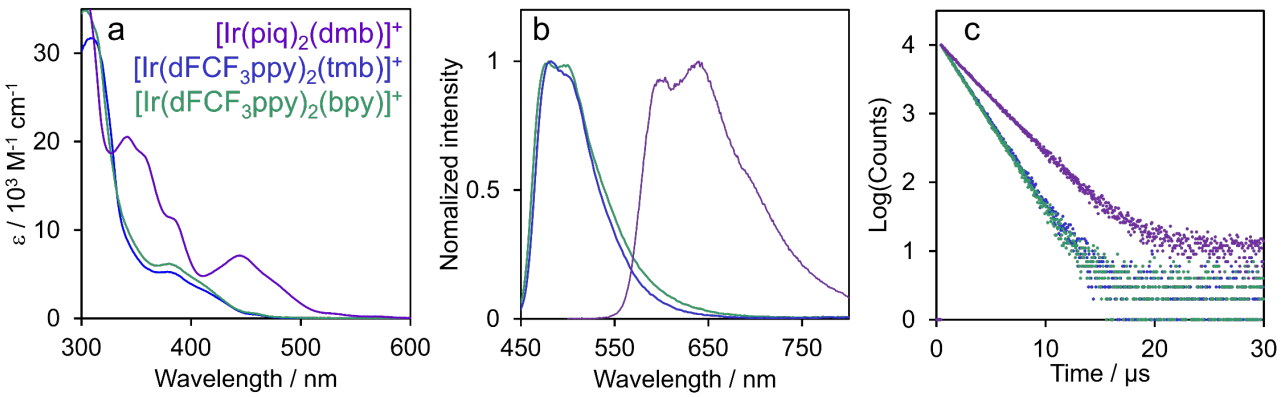

Fig. S6. (a) UV-vis absorption and (b) emission spectra, and (c) lifetimes (τ_{em}) of **[Ir(C^N)$_2$(N^N)]$^+$** in DMA at room temperature.

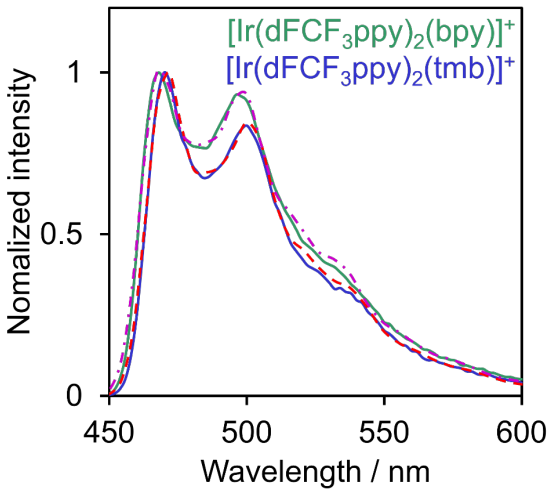

Fig. S7. Franck–Condon analyses based on the emission spectra of **[Ir(C^N)$_2$(N^N)]$^+$** in DMA at low temperature.

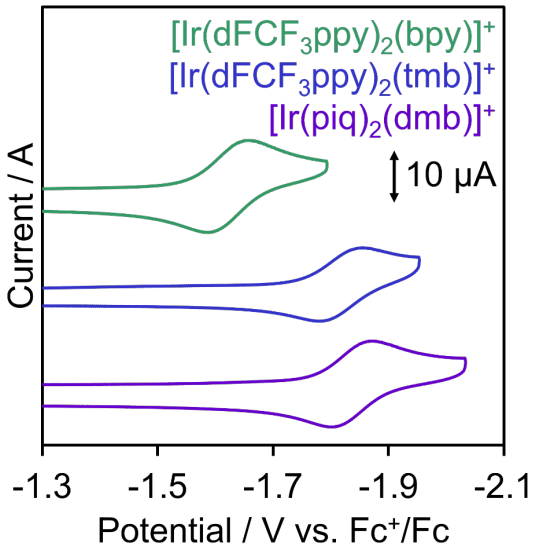

Fig. S8. Cyclic voltammograms of **[Ir(C^N)$_2$(N^N)]$^+$** (0.5 mM) acquired in Ar–saturated DMA containing Et_4NBF_4 (0.1 M) using a glassy-carbon working (diameter, 3 mm) and Pt-wire counter electrodes at a scan rate of 200 mV s^{-1}.

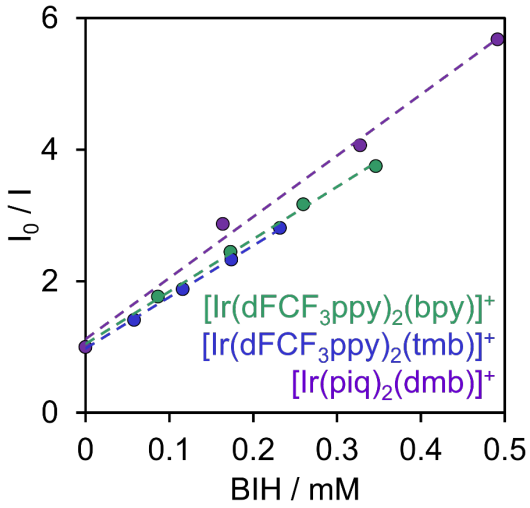

Fig. S9. Stern–Volmer plots of **[Ir(C^N)$_2$(N^N)]$^+$** in DMA in the presence of BIH at various concentrations.

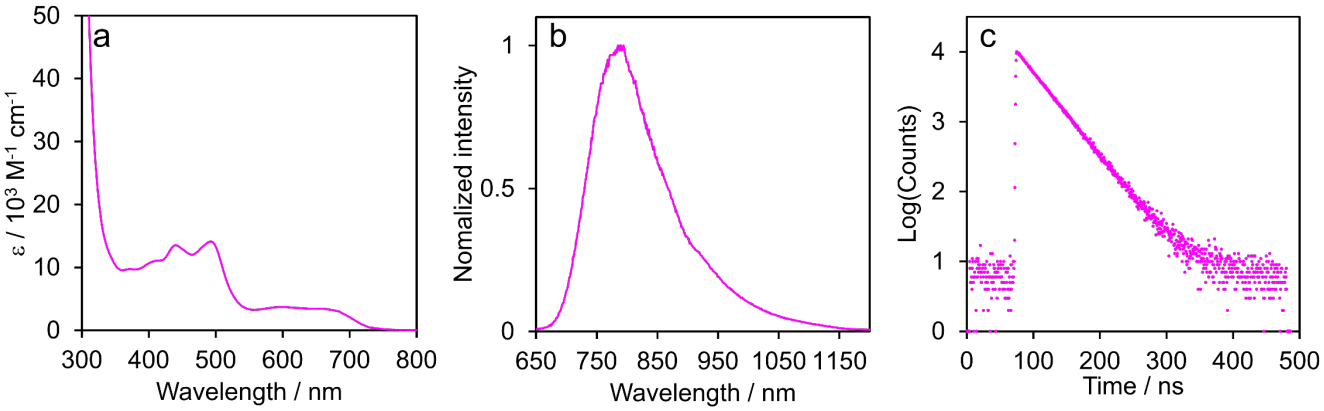

Fig. S10. (a) UV-vis absorption and (b) emission spectra, and (c) lifetimes (τ_{em}) of **[Os(CF$_3$bpy)$_3$]$^{2+}$** in DMA.

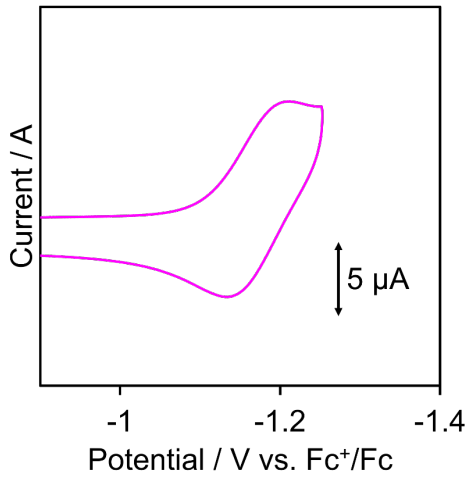

Fig. S11. Cyclic voltammogram of **[Os(CF$_3$bpy)$_3$]$^{2+}$** (0.5 mM) acquired in Ar−saturated DMA containing Et_4NBF_4 (0.1 M) using glassy-carbon working (diameter, 3 mm) and Pt-wire counter electrodes at a scan rate of 200 mV s^{-1}.

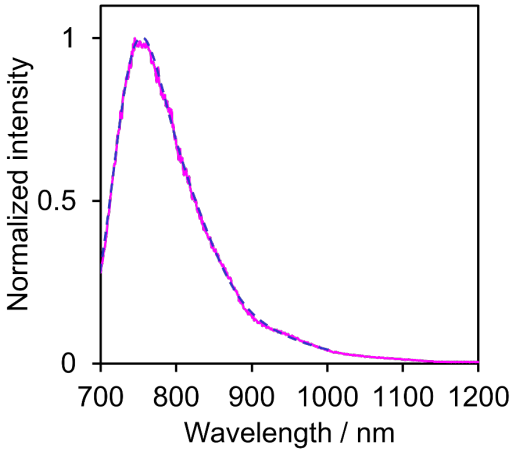

Fig. S12. Franck–Condon analysis based on the emission spectrum of **[Os(CF$_3$bpy)$_3$]$^{2+}$** in DMA at a low temperature. The broken blue line corresponds to the Franck–Condon-fitted curve.

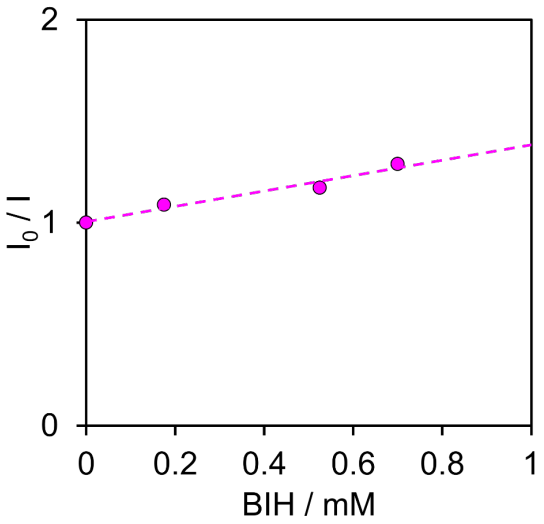

Fig. S13. Stern−Volmer plot for **[Os(CF$_3$bpy)$_3$]$^{2+}$** in DMA in the presence of BIH of various concentrations.

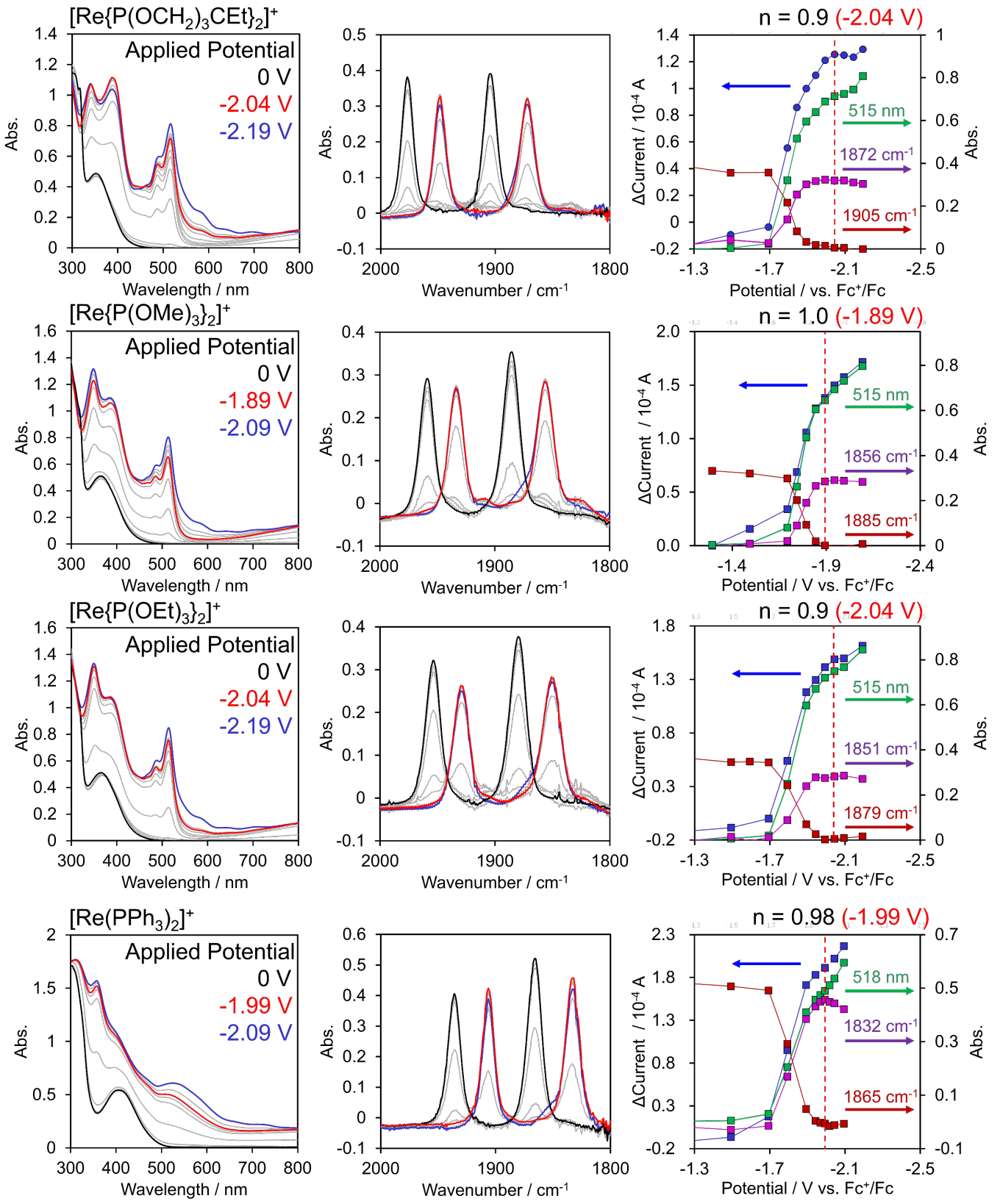

Fig. S14. UV–vis (left) and FT-IR (centre) absorption spectra acquired for each reduced $[Re(PR_3)_2]^+$ by flow electrolysis. Dependences of current and absorption on applied voltage (right). Each two-electron-reduced $[Re(PR_3)_2]^+$ species exhibited UV-vis absorption at an applied potential that corresponds to about one electron (n = 1.0). Therefore, the molar extinction coefficients of each OERS were determined from the change in the UV-vis spectrum and the ground-state attenuation in the FTIR spectrum observed at the applied potential where the absorption of the two-electron-reduced species is not observed.

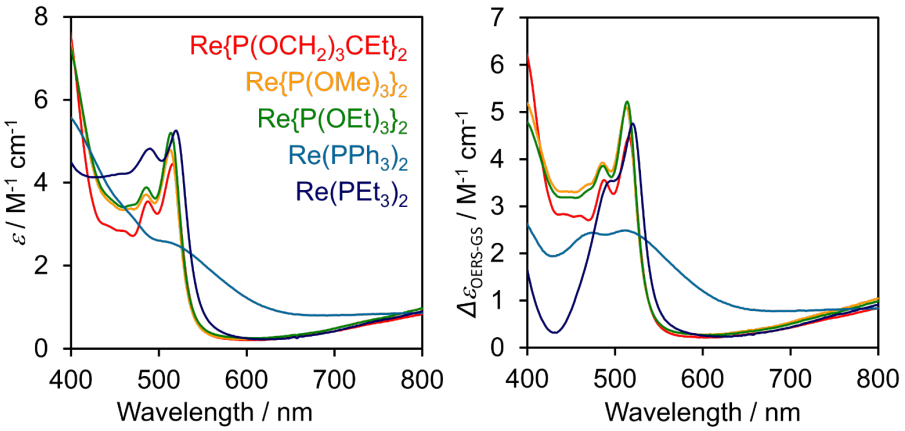

Fig. S15. Molar extinction coefficients of the OERSs of $[Re(PR_3)_2]^+$ as functions of wavelength (left) and OERS/ground-state differences determined by flow electrolysis.

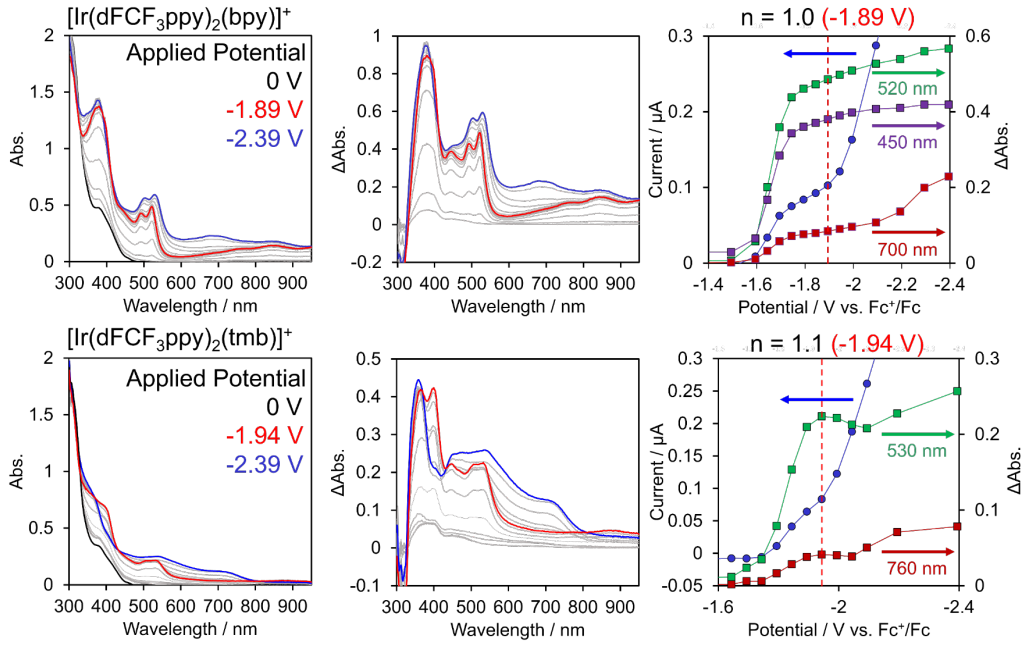

Fig. S16. UV–vis absorption spectra of each reduced $[Ir(C^N)_2(N^N)]^+$ obtained by flow electrolysis, and dependences of current and absorption on applied voltage (right).

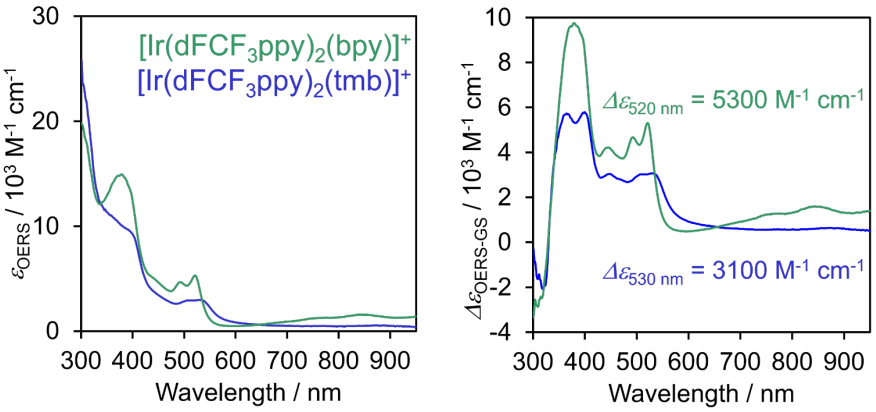

Fig. S17. Molar extinction coefficients of the OERSs of $[Ir(C^N)_2(N^N)]^+$ (left) and OERS/ground-state differences determined by flow electrolysis.

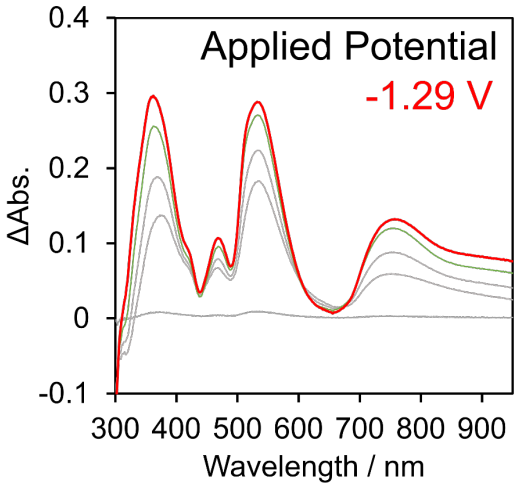

Fig. S18. UV–vis absorption difference spectra of reduced $[Os(CF_3bpy)_3]^{2+}$ obtained by flow electrolysis. Isosbestic points were not observed at 600 and 680 nm; however, they were observed in OTTLE experiments (Fig. S19) and when OERSs were generated by irradiation with light (Fig. S23). This strange absorption is possibly ascribable to interactions between the reduced species of $[Os(CF_3bpy)_3]^{2+}$ and oxygen molecules introduced by leaks in the flow electrolysis instrument.

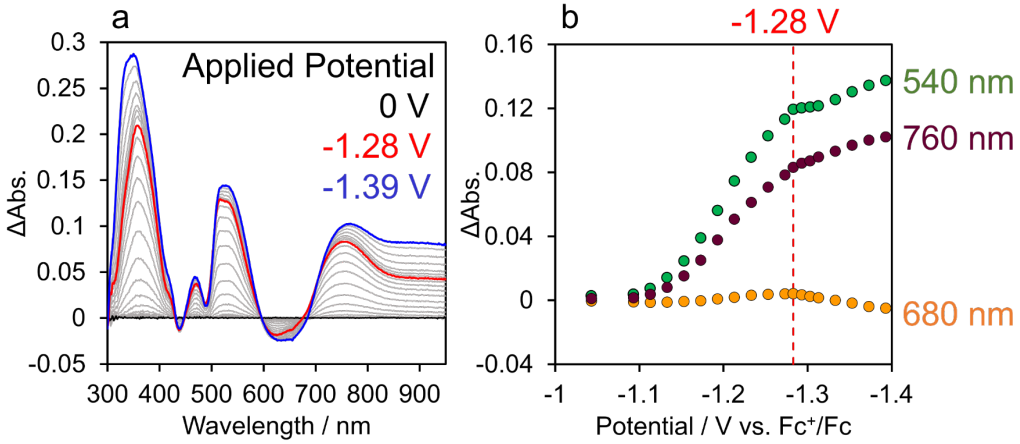

Fig. S19. (a) UV–vis absorption difference spectra of the OERS of $[Os(CF_3bpy)_3]^{2+}$ obtained using the optically transparent thin-layer electrochemical (OTTLE) method, and (b) dependences of absorption on applied voltage. The UV-vis absorption spectrum of the OERS of $[Os(CF_3bpy)_3]^{2+}$ obtained from the spectrum at an applied potential of −1.28 V vs. Fc^+/Fc is shown in red.

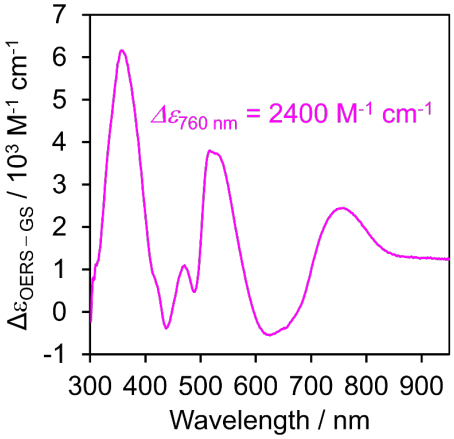

Fig. S20. Difference in the molar extinction coefficients of the OERS and ground state of $[Os(CF_3bpy)_3]^{2+}$ as a function of wavelength, as determined by the OTTLE experiment.

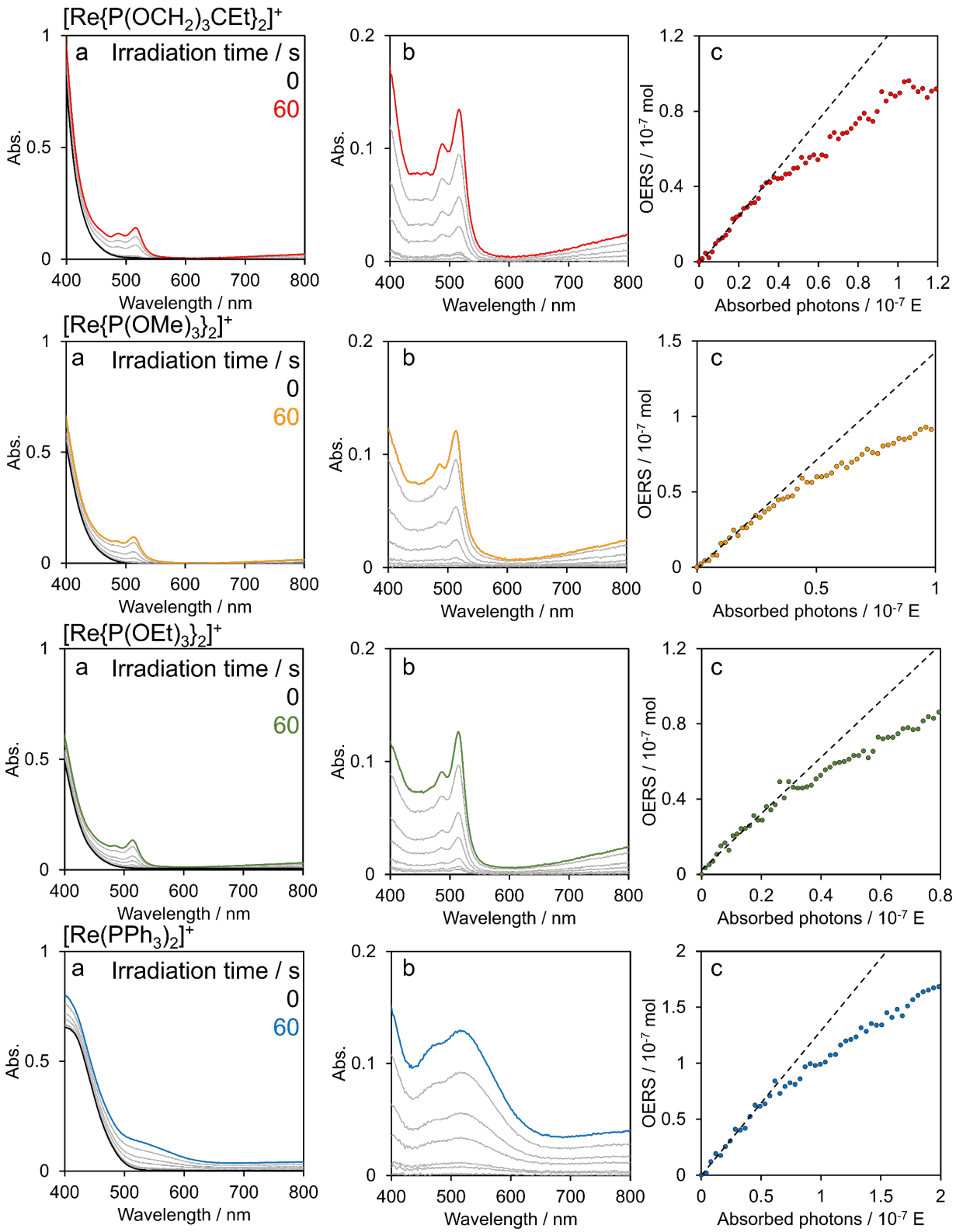

Fig. S21. (a) Visible absorption changes observed for Ar–saturated DMA solutions of **[Re(PR$_3$)$_2$]$^+$** and BIH (0.1 M) when irradiated with light at λ_{ex} = 436 nm. The concentration of the complex was 0.5 mM and the light intensity was 6.1 x 10^{-9} E s^{-1} for **[Re{P(OCH$_2$)$_3$CEt}$_2$]$^+$**. The concentration of the complex was 0.2 mM and light intensity was 6.2 x 10^{-9} E s^{-1} for In **[Re{P(OMe)$_3$}$_2$]$^+$**. The concentration of the complex was 0.2 mM and light intensity was 4.7 x 10^{-9} E s^{-1} for **[Re{P(OEt$_3$)$_2$}]$^+$**. The concentration of the complex was 0.2 mM and light intensity was 6.1 x 10^{-9} E s^{-1} for **[Re(PPh$_3$)$_2$]$^+$**. (b) Difference absorption spectra before/after irradiation with light. (c) Relationship between the number of absorbed photons and the concentration of the OERS of **[Re(PR$_3$)$_2$]$^+$** in solution.

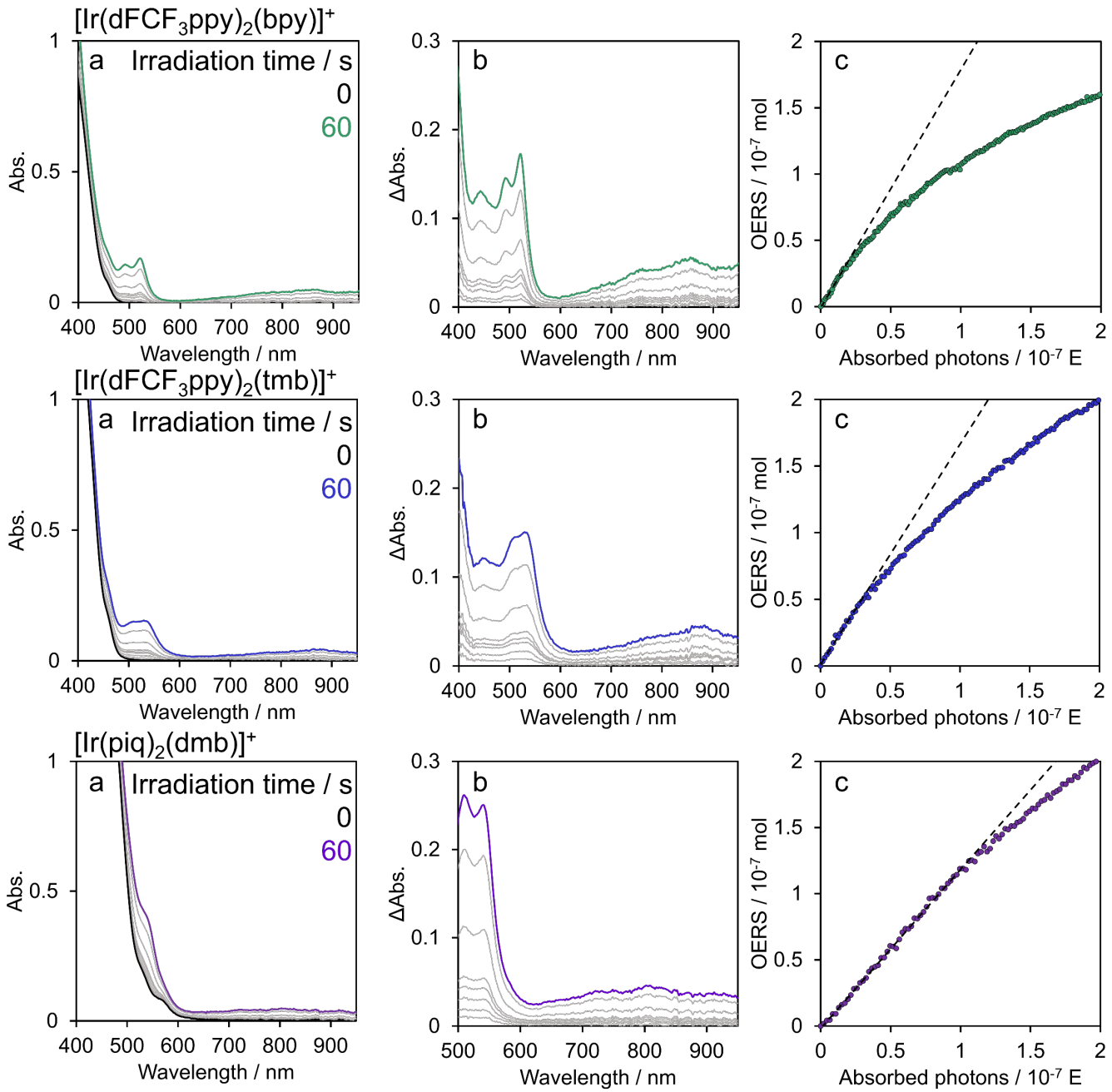

Fig. S22. (a) Visible absorption changes observed for Ar–saturated DMA solutions containing **[Ir(dFCF$_3$ppy)$_2$(bpy)]$^+$** (0.2 mM), **[Ir(dFCF$_3$ppy)$_2$(tmb)]$^+$** (0.5 mM), or **[Ir(piq)$_2$(dmb)]$^+$** (0.3 mM) with BIH (0.1 M) during irradiation with light at λ_{ex} = 436 nm (4.4 x 10^{-9} E s^{-1}) and (b) difference absorption spectra before/after irradiation with light. (c) Relationships between the number of absorbed photons and the number of **[Ir(C^N)$_2$(N^N)]$^+$** OERSs in solution. The number of **[Ir(piq)$_2$(dmb)]$^+$** OERSs was calculated using the reported molar extinction coefficient of OERS (ε_{OER}).[10]

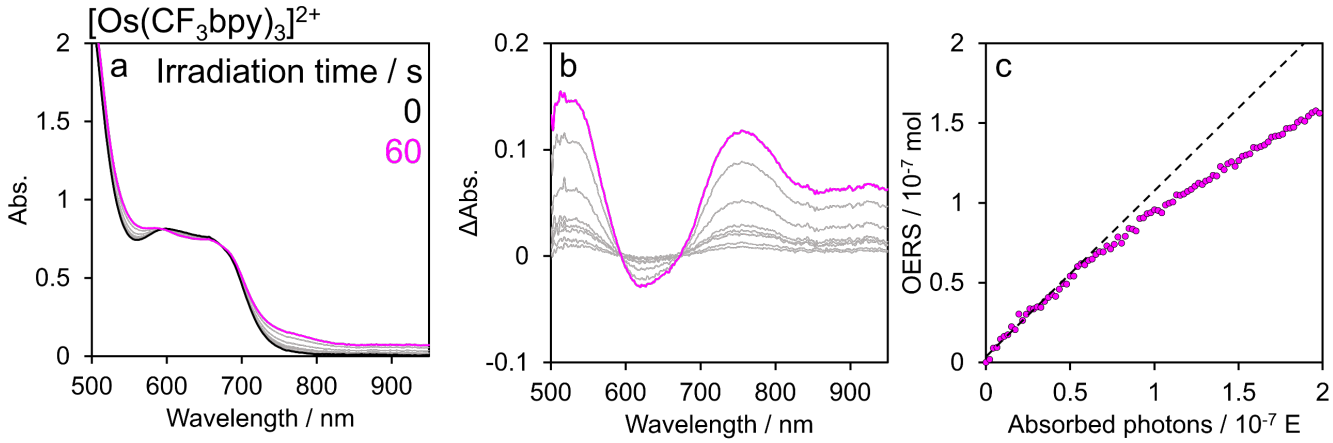

Fig. S23. (a) Visible absorption changes of an Ar–saturated DMA solution containing **[Os(CF$_3$bpy)$_3$]$^{2+}$** (0.2 mM) and BIH (0.1 M) during irradiation with light at λ_{ex} = 436 nm (5.2 x 10^{-9} E s^{-1}) and (b) difference absorption spectra before/after irradiation with light. (c) Relationship between the number of absorbed photons and the **[Os(CF$_3$bpy)$_3$]$^{2+}$** OERS concentration in solution.

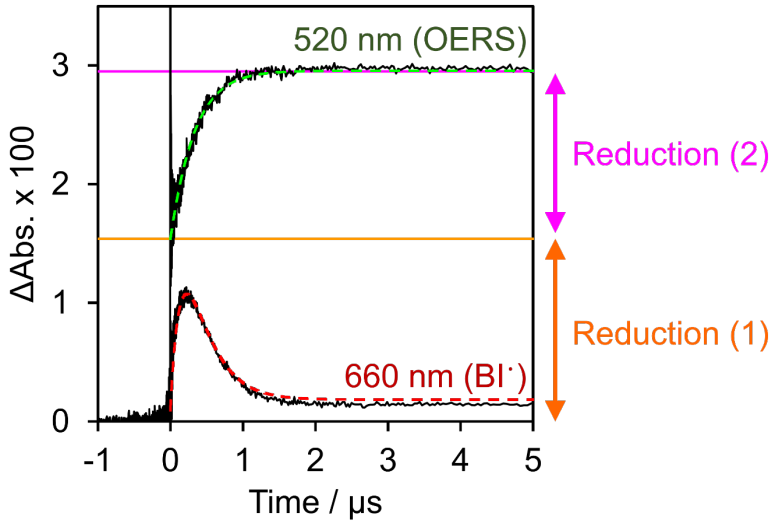

Fig. S24. Transient absorption spectroscopy of a DMA solution containing **[Re(PEt$_3$)$_2$]$^+$** (1.0 mM) and BIH (0.1 M) at an excitation wavelength of 532 nm. The black traces correspond to absorbance-difference (ΔAbs.) changes (upper: 520 nm, lower: 660 nm). The green curve is fitted to ΔAbs. changes at 520 nm, while the red curve corresponds to fitted ΔAbs. changes at 660 nm. The orange line shows ΔAbs. at 520 nm at the completion of reduction (1), while the pink line shows ΔAbs. at 520 nm at the completion of reduction (2). ΔAbs. at 520 nm primarily reflects changes in the concentration of OERS of **[Re(Pet$_3$)$_2$]$^+$**, while ΔAbs. at 660 nm primarily reflects changes in the concentration of BI$^\bullet$. Because ΔAbs. at 520 nm at the completion of the first reduction could not be determined due to the influence of scattered light, it was determined by fitting ΔAbs. changes at 520 nm and 660 nm. By determining the concentrations of OERS and BI$^\bullet$ based on the following differential equations (Eqs. IV-VI) and applying fitting analysis using the molar extinction coefficient of OERS obtained from flow electrolysis (Fig. 5), the molar extinction coefficients of BI$^\bullet$ at 520 and 660 nm, as well as the rate constant for electron transfer from BI$^\bullet$ to PS (k_{et}), were determined. The following reported rate constants were used during fitting: deprotonation of BIH$^{\bullet+}$ (k_{dp} = 6.1×10^7 s^{-1}) and back-electron-transfer between free radical ions (k_{rec} = 9.5×10^9 s^{-1}) in a DMA solution.[11]

$$\frac{d[BIH^{\bullet+}]}{dt} = -(k_{dp}[BIH] + k_{rec}[PS^{\bullet-}])[BIH^{\bullet+}] \quad \text{(IV)}$$

$$\frac{d[BI^{\bullet}]}{dt} = k_{dp}[BIH][BIH^{\bullet+}] - k_{et}[PS][BI^{\bullet}] \quad \text{(V)}$$

$$\frac{d[PS^{\bullet-}]}{dt} = k_{et}[PS][BI^{\bullet}] - k_{rec}[BIH^{\bullet+}][PS^{\bullet-}] \quad \text{(VI)}$$

As a result of the fitting, the molar extinction coefficient of $BI^{\bullet}$ at 520 nm was determined to be 2000 M^{-1} cm^{-1}, at 660 nm to be 5500 M^{-1} cm^{-1}, and k_{et} was determined to be 3.2 $\times 10^9$ M^{-1} s^{-1}. The ratio of reduction (1) to reduction (2) was 52:48.

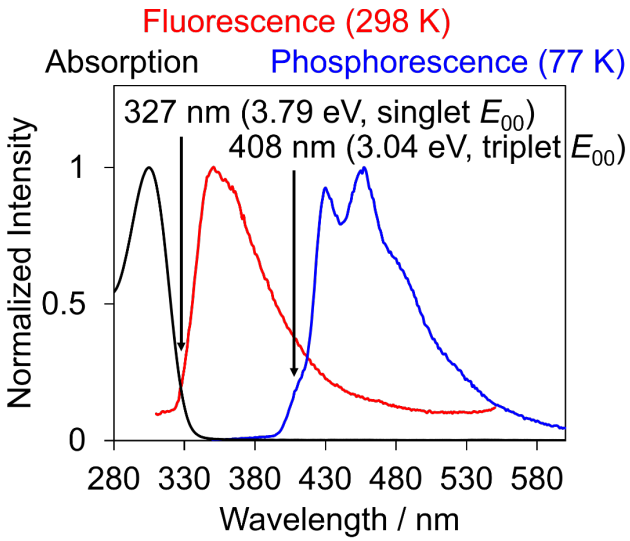

Fig. S25. Absorption (black, measured at 298 K), fluorescence (red, measured at 298 K), and phosphorescence (blue, measured at 77 K) spectra of BIH (all were measured in DMA). The 0-0 transition energy of S_0-S_1 (E_{00} of the singlet excitation) was determined as 3.79 eV from the wavelength (327 nm) where the absorption and fluorescence spectra were overlapped. E_{00} of the S_0-T_1 excitation was determined as 3.04 eV (λ = 408 nm) where the highest-energy band was observed.

Table S1. Results of Franck-Condon analysis[a]

Complex	$\tilde{\nu}_{00}$ / cm^{-1}	$\tilde{\nu}_{1/2}$ / cm^{-1}	ν_M / cm^{-1}	S_M	ν_L / cm^{-1}	S_L
$[Re\{P(OCH_2)_3CEt\}_2]^+$	20900	1390	1450 [b]	1.4	760	1.3
$[Re\{P(OMe)_3\}_2]^+$	19600	1800	1450 [b]	1.6	490	1.1
$[Re\{P(OEt)_3\}_2]^+$	20100	1390	1450 [b]	1.1	780	2.4
$[Re(PPh_3)_2]^+$	19300	1230	1450 [b]	0.57	870	2.2
$[Re(PEt_3)_2]^+$	17500	1440	1450 [b]	0.93	470	2.7
$[Ir(dFCF_3ppy)_2(bpy)]^+$	21400	710	1330	0.99	680	0.80
$[Ir(dFCF_3ppy)_2(tmb)]^+$	21300	710	1330	0.93	710	0.70
$[Os(CF_3bpy)_3]^{2+}$	14100	660	1890	0.36	490	2.8

[a] Using emission spectra measured at 77 K. [b] Fixed value of 1450 cm^{-1} cited from ref. 12

Reference

1 K. Koike, J. Tanabe, S. Toyama, H. Tsubaki, K. Sakamoto, J. R. Westwell, F. P. Johnson, H. Hori, H. Saitoh and O. Ishitani, New Synthetic Routes to Biscarbonylbipyridinerhenium(I) Complexes *cis,trans*-$[Re(X_2bpy)(CO)_2(PR_3)(Y)]^{n+}$ (X_2bpy = 4,4'-X_2-2,2'-bipyridine) via Photochemical Ligand Substitution Reactions, and Their Photophysical and Electrochemical Properties, *Inorg. Chem.*, 2000, **39**, 2777-2783.

2 T. Morimoto, M. Ito, K. Koike, T. Kojima, T. Ozeki and O. Ishitani, Dual Emission from Rhenium(I) Complexes Induced by an Interligand Aromatic Interaction, *Chem. Eur. J.*, 2012, **18**, 3292-3304.

3 S. J. Liu, Q. Zhao, Q. L. Fan and W. Huang, A Series of Red-Light-Emitting Ionic Iridium Complexes: Structures, Excited State Properties, and Application in Electroluminescent Devices, *Eur. J. Inorg. Chem.*, **2008**, 2177-2185.

4 P. Delgado, R. J. Glass, G. Geraci, R. Duvadie, D. Majumdar, R. I. Robinson, I. Elmaarouf, M. Mikus and K. L. Tan, Use of Green Solvents in Metallaphotoredox Cross-Electrophile Coupling Reactions Utilizing a Lipophilic Modified Dual Ir/Ni Catalyst System, *J. Org. Chem.*, 2021, **86**, 17428-17436.

5 E. Hasegawa, T. Seida, N. Chiba, T. Takahashi and H. Ikeda, Contrastive Photoreduction Pathways of Benzophenones Governed by Regiospecific Deprotonation of Imidazoline Radical Cations and Additive Effects, *J. Org. Chem.*, 2005, **70**, 9632-9635.
6 J. L. Smithback, J. B. Helms, E. Schutte, S. M. Woessner and B. P. Sullivan, Preparative Routes to Luminescent Mixed-Ligand Rhenium(I) Dicarbonyl Complexes, *Inorg. Chem.*, 2006, **45**, 2163-2174.
7 G. H. Allen, R. P. White, D. P. Rillema and T. J. Meyer, Synthetic Control of Excited-State Properties. Tris-Chelate Complexes Containing the Ligands 2,2'-Bipyrazine, 2,2'-Bipyridine, and 2,2'-Bipyrimidine, *J. Am. Chem. Soc.*, 1984, **106**, 2613-2620.
8 K. Huang and A. Rhys, Theory of Light Absorption and Non-Radiative Transitions in F-Centres, *Proc. R. Soc. Lond. A*, 1950, **204**, 406-423.
9 C. G. Hatchard and C. A. Parker, A New Sensitive Chemical Actinometer - II. Potassium Ferrioxalate as a Standard Chemical Actinometer, *Proc. R. Soc. Lond. A*, 1956, **235**, 518-536.
10 Y. Kuramochi and O. Ishitani, Iridium(III) 1-Phenylisoquinoline Complexes as a Photosensitizer for Photocatalytic CO_2 Reduction: A Mixed System with a Re(I) Catalyst and a Supramolecular Photocatalyst, *Inorg. Chem.*, 2016, **55**, 5702-5709.
11 K. Ozawa, Y. Tamaki, K. Kamogawa, K. Koike and O. Ishitani, Factors determining formation efficiencies of one-electron-reduced species of redox photosensitizers, *J. Chem. Phys.*, 2020, **153**, 154302
12 J. V. Caspar, T. D. Westmoreland, G. H. Allen, P. G. Bradley, T. J. Meyer and W. H. Woodruff, Molecular and Electronic Structure in the Metal-to-Ligand Charge-Transfer Excited States of d^6 Transition-Metal Complexes in Solution, *J. Am. Chem. Soc.*, 1984, **106**, 3492-3500.